

May 29, 2020

Impact of eccentricity on the gravitational wave searches for binary black holes: High mass caseAntoni Ramos-Buades,¹ Shubhanshu Tiwari,² Maria Haney,² and Sascha Husa¹¹*Departament de Física, Universitat de les Illes Balears, IAC3 – IEEC, Crta. Valldemossa km 7.5, E-07122 Palma, Spain*²*Physik-Institut, Universität Zürich, Winterthurerstrasse 190, 8057 Zürich, Switzerland*

The possible formation of stellar-mass binary black holes through dynamical interactions in dense stellar environments predicts the existence of binaries with non-negligible eccentricity in the frequency band of ground-based gravitational wave detectors; the detection of binary black hole mergers with measurable orbital eccentricity would validate the existence of this formation channel. Waveform templates currently used in the matched-filter gravitational-wave searches of LIGO-Virgo data neglect effects of eccentricity which is expected to reduce their efficiency to detect eccentric binary black holes. Meanwhile, the sensitivity of coherent unmodeled gravitational-wave searches (with minimal assumptions about the signal model) have been shown to be largely unaffected by the presence of even sizable orbital eccentricity. In this paper, we compare the performance of two state-of-the-art search algorithms recently used by LIGO and Virgo to search for binary black holes in the second Observing Run (O2), quantifying their search sensitivity by injecting numerical-relativity simulations of inspiral-merger-ringdown eccentric waveforms into O2 LIGO data. Our results show that the matched-filter search PyCBC performs better than the unmodeled search cWB for the high chirp mass ($> 20M_\odot$) and low eccentricity region ($e_{30\text{Hz}} < 0.3$) of parameter space. For moderate eccentricities and low chirp mass, on the other hand, the unmodeled search is more sensitive than the modeled search.

PACS numbers: 04.25.Dg, 04.25.Nx, 04.30.Db, 04.30.Tv

I. INTRODUCTION

The number of detections of gravitational wave (GW) signals has steeply increased from the first and second Observing runs (O1/O2) of Advanced LIGO and Advanced Virgo [1] to the third Observing run (O3), where tens of GW candidates have already been recorded [2–5]. So far, all GW detections of binary black holes (BBHs) are consistent with signals emitted from quasicircular binaries [6, 7].

Generally, two main scenarios can be considered regarding possible formation channels for BBH mergers: 1) isolated binary evolution [8–11], during which BBHs shed their formation eccentricity through GW emission and have circularized by the time they enter the frequency band of the ground-based detectors [12, 13]; 2) binaries dynamically formed in dense stellar environments like globular clusters and active galactic nuclei [14–18], which may still retain a significant eccentricity by the time they enter the frequency band of the Advanced LIGO [19] and Advanced Virgo [20] detectors. Although both formation channels (and their different astrophysical scenarios) predict BBH mergers with distinct distributions of masses and spins [21–24], the model uncertainties—as well as the low statistics due to the limited number of GW detections—do not permit to set tight constraints on BBH formation scenarios from the mass and spin distributions alone.

Dynamical BBH formation, however, is distinctly characterized by the potential existence of binaries with non-negligible eccentricity in the frequency band of the ground-based detectors, which were formed through dynamical capture at very close separations (without time to circularize before merger) or through a dynamical process that increased the eccentricity of the binary (e.g. Kozai-Lidov oscillations [25, 26]). The detection of a GW signal with an unambiguous signature of non-negligible orbital eccentricity would there-

fore confirm the dynamical formation channel for BBHs and provide information about possible formation mechanisms and the astrophysical environments of such sources.

In order to be able to confidently detect eccentric binary black hole signals it is necessary to assess the sensitivity of the pipelines used to search for such signals. As a consequence several studies have analysed the sensitivity of different search pipelines to eccentric compact binary mergers over data from O1 and O2 Advanced LIGO and Advanced Virgo observing runs [27–29].

In this paper we quantify the sensitivity of two different gravitational-wave search pipelines to eccentric inspiral-merger-ringdown (IMR) signals calculated from numerical relativity (NR) simulations. The two search pipelines are: 1) the template-based PyCBC algorithm [30, 31], and 2) the unmodeled coherent WaveBurst (cWB) algorithm [32, 33]. We study the sensitivity of the pipelines with increasing eccentricity of the signal for three different mass ratios $q = 1, 2, 4$, with $q = m_1/m_2 > 1$ and m_1, m_2 the component masses of the binary. Furthermore, for mass ratio $q = 1$ we inject eccentric simulations with increasing dimensionless component spins $|\vec{\chi}_i| \leq 0.75$ (aligned with the orbital angular momentum of the system), where $\vec{\chi}_i = \vec{S}_i/m_i^2$ and \vec{S}_i the spin vector of the i -component, with $i = 1, 2$. Due to the restricted length of the NR simulations the waveforms are injected at a start frequency of 30Hz, and the eccentricity is consistently defined at that frequency according to the procedure detailed in Sec. II.

The paper is organised as follows: In Sec. II we provide details about the IMR NR eccentric waveforms used in this work. In Sec. III we briefly summarize the two search algorithms considered in this study, the template-based search PyCBC and the un-modeled search, cWB. We present in Sec. IV the results of the sensitivity estimates of both studied pipelines. We conclude in Sec. V discussing the results obtained and reporting our conclusions.

II. ECCENTRIC BINARY BLACK HOLES

The gravitational wave signals emitted from generic binary black holes are described by 17 parameters [34]. The parameters of a binary can be separated into 10 intrinsic parameters, i.e. properties of the emitting source, and 7 extrinsic parameters, describing the position of the source in the detector sky. The intrinsic parameters are the two component masses m_i , the six dimensionless spin vectors $\vec{\chi}_i = \vec{S}_i/m_i^2$, the eccentricity parameter e , and the argument of the periastris Ω . Another useful mass parameter in gravitational wave data analysis is the chirp mass \mathcal{M} of a binary with masses m_1 and m_2 , which is defined as $\mathcal{M} \equiv (m_1 m_2)^{3/5} (m_1 + m_2)^{-1/5}$.

The extrinsic parameters are the luminosity distance d_L , the azimuthal angle φ , the inclination ι , the time of coalescence t_c , the polarization angle ψ , the right ascension ϕ and the declination θ . The strain induced in a gravitational wave detector can be written in terms of these parameters as [35, 36]

$$h(t, \zeta, \Theta) = F_+(\theta, \phi, \psi) h_+(t - t_c; \iota, \varphi, \zeta) + F_\times(\theta, \phi, \psi) h_\times(t - t_c; \iota, \varphi, \zeta), \quad (2.1)$$

where F_+ , F_\times are the antenna pattern functions, and $\Theta = \{t_c, r, \theta, \varphi, \psi, \iota, \phi\}$ and $\zeta = \{m_1, m_2, \vec{S}_1, \vec{S}_2, e, \Omega\}$ represent the sets of extrinsic and intrinsic parameters, respectively. The gravitational wave polarizations (h_+ , h_\times) appearing in the detector response can be expressed as a complex waveform strain

$$h(t) = h_+ - i h_\times = \sum_{l=2}^{\infty} \sum_{m=-l}^l Y_{lm}^{-2}(\iota, \varphi) h_{lm}(t - t_c; \zeta), \quad (2.2)$$

where h_{lm} are the (l, m) waveform modes and $Y_{lm}^{-2}(\iota, \varphi)$ the spherical harmonics of spin-weight -2 .

A. Numerical Relativity data set

In this work we inject eccentric NR waveforms produced with the open-source EinsteinToolkit (ET) code [37, 38] and the SpEc code [39]. The ET waveforms were presented in [40], and the SXS ones in [41]. The injected waveforms are displayed in Table I, where we show for each simulation its identifier (ID, an integer number), the simulation name, mass ratio, z-components of the dimensionless spin vectors ($\chi_{1,z}, \chi_{2,z}$) and the initial eccentricity measured with the method developed in [40].

The injected data set is chosen with the following criteria: simulations with IDs 1 – 4 are equal mass non-spinning cases which serve as control cases because eccentric equal mass non-spinning binaries have already been studied in the literature [42], while simulations with IDs 5 – 10 extend the equal mass case to the spinning sector. Finally, simulation sets 11 – 14 and 15 – 17 allow to test the efficiency of the pipelines at higher mass ratios without including spin effects.

The eccentricity parameter describes the ellipticity of the binary's orbit, values close to 0 indicate a quasi-circular evolution while values close to 1 represent an almost head-on col-

ID	Simulation	q	$\chi_{1,z}$	$\chi_{2,z}$	e_0^{NR}
1	SXS:BBH:1356	1.	0.	0.	0.09
2	SXS:BBH:1360	1.	0.	0.	0.15
3	SXS:BBH:1363	1.	0.	0.	0.23
4	Eccq1.---0.---0.---et0.5.D27	1.	0.	0.	0.30
5	Eccq1.---0.25---0.25---et0.1.D14	1.	-0.25	-0.25	0.07
6	Eccq1.---0.5---0.5---et0.1.D13	1.	-0.5	-0.5	0.07
7	Eccq1.---0.75---0.75---et0.1.D13	1.	-0.75	-0.75	0.08
8	Eccq1.---0.25---0.25---et0.2.D16	1.	0.25	0.25	0.12
9	Eccq1.---0.5---0.5---et0.2.D15	1.	0.5	0.5	0.12
10	Eccq1.---0.75---0.75---et0.2.D15	1.	0.75	0.75	0.12
11	SXS:BBH:1365	2.	0.	0.	0.06
13	Eccq2.---0.---0.---et0.2.D16	2.	0.	0.	0.14
12	SXS:BBH:1369	2.	0.	0.	0.20
14	Eccq2.---0.---0.---et0.5.D26	2.	0.	0.	0.30
15	Eccq4.---0.---0.---et0.1.D12	4.	0.	0.	0.07
16	Eccq4.---0.---0.---et0.2.D15	4.	0.	0.	0.14
17	Eccq4.---0.---0.---et0.5.D27.5	4.	0.	0.	0.30

Table I: Summary of the injected NR simulations. The first column denotes the identifier of the simulation, the second column indicates the name of the simulation as presented in [40, 41]. Next columns show the mass ratio, z-component of the dimensionless spin vectors and the initial NR eccentricity as measured using the procedure detailed in [40].

lision. In general relativity the eccentricity is a gauge dependent quantity. As a consequence, a plethora of eccentricity estimators have been developed to measure the eccentricity in numerical relativity simulations [43–49]. Eccentricity estimators are combinations of dynamical or wave quantities, like the orbital frequency of the binary, the orbital separation, the gravitational wave frequency of the $(2, 2)$ mode, etc., measuring the relative oscillations in those quantities due to eccentricity. In this work we measure the eccentricity from the gravitational wave frequency of the h_{22} mode, ω_{22} , following the procedures of [40]. We remark that the eccentricities presented in Table I are measured from the gravitational wave frequency and their values differ from those presented in [40] as they were calculated there using the orbital frequency computed from the trajectories of the black holes.

In the top panel of Fig. 1 we show the time evolution of the eccentricity of the simulation with ID 17 in Table I. Moreover, we choose the end of the inspiral given by the minimum energy circular orbit (MECO) [50], and explicitly set the eccentricity to zero from the MECO time onwards as at that point the eccentricity is so small which is practically zero.

In this study we are interested in injecting the waveforms presented in Table I at a certain detector frequency and for a certain total mass distribution. The modification of the total mass of the system implies a change in length of the waveform within the frequency band of the detector, as a consequence different total masses imply also different initial eccentricities, as one can appreciate from the top panel of Fig. 1, which shows the eccentricity as a monotonically decaying

function as the binary evolves. One possible solution might be to express the eccentricity measured from the NR simulation as a function of gravitational wave frequency of the 22-mode scaled by the total mass of the system, $2\pi M f_{22} = M\omega_{22}$, approximate the value of the injection frequency by the frequency of the 22-mode, $f_{22} \approx f_{\text{GW}}$, and construct a function $e(M f_{\text{GW}})$ which would provide the value of the eccentricity at a certain total mass for a given injection frequency. However, in the eccentric case the gravitational wave frequency is a non-monotonic function due to the asymmetric gravitational interaction along the orbit of the binary as one can observe in the mid panel of Fig. 1, where the time domain frequency of the 22-mode for the eccentric simulation with ID 17 from Table I and the frequency of the quasicircular IMRPhenomT [51] waveform model for the same configuration are displayed. We note that after the MECO time both curves converge indicating circularization of the eccentric system at merger.

One possibility for the definition of the eccentricity as a function of a monotonically increasing frequency is to consider the post-Newtonian (PN) approximation, and use the Radiation Reaction (RR) equations [52] for the PN parameter, x , which can be written in terms of the orbital frequency, $x = \omega^{2/3}$, and the temporal eccentricity¹ e_t . The RR equations are ordinary differential equations for the temporal evolutions of x and e_t , derived from the angular momentum and gravitational wave energy fluxes [52]. In practice, in the RR equation for e_t one could replace it by the eccentricity measured from the NR simulation and solve the differential equation for \dot{x} . However, we find that this procedure does not work satisfactorily, as we have checked that the RR equations show a divergent behavior before the MECO time in some cases, indicating the breakdown of the post-Newtonian approximation. Therefore, we decide to take the gravitational wave frequency of IMRPhenomT and combine it with the eccentricity measured from the simulation to construct the function $e_{\text{NR}}(M f_{22})$. The outcome of such a calculation for the simulation with ID 17 in Table I is shown in the bottom plot of Fig. 1. Hence, given an injection with total mass M_T and an injection frequency of f_{GW} , we can compute the eccentricity at that frequency and total mass as

$$e_{\text{inj}} = e_{\text{NR}}(M_T f_{\text{GW}}). \quad (2.3)$$

We note that we focus only on the eccentricity parameter as the initial argument of the periastris² in the non-precessing case acts as an initial phase during the inspiral. Its main impact is in the morphology of the waveform at plunge, whose detailed study would require going beyond the maximum total mass considered in this communication ($M_T > 100M_\odot$). We leave for future work analyzing such high total mass regime.

Finally, in Fig. 2 we plot the time evolution of the GW polarization state $h_x(t)$ for non-spinning, eccentric stellar-mass

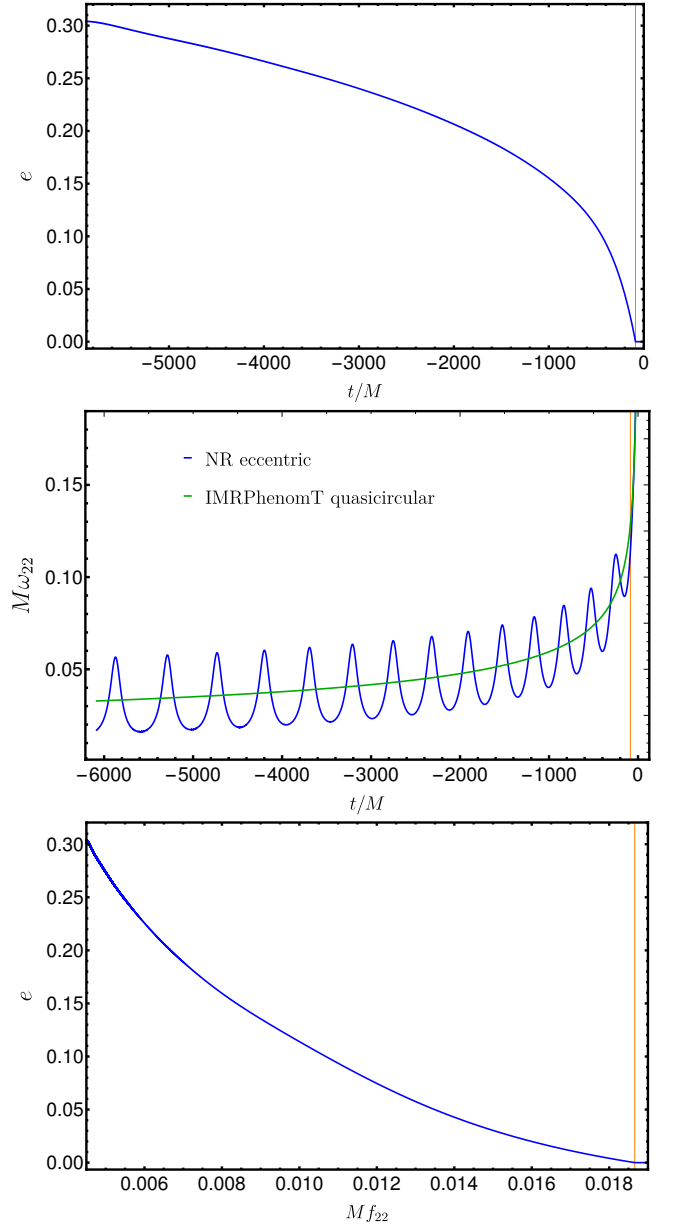


Figure 1: Top panel: Time domain evolution of the eccentricity estimated from the eccentric NR simulation with ID 17 in Table I. Mid panel: Time domain 22-mode gravitational wave frequencies of the eccentric case with ID 17 from Table I and of the quasicircular IMRPhenomT waveform model, highlighted in blue and green colors respectively. Bottom panel: Eccentricity as a function of the gravitational frequency of the (2, 2) mode for the same configuration as in the upper panel. With vertical lines in the top and bottom plots we have highlighted the MECO time and frequency, respectively.

binary black holes with total mass $M_T = 50M_\odot$ and mass ratio $q = 2$, provided by numerical-relativity simulations. The characteristic orbital eccentricity of the system —defined at a reference frequency of 30Hz —is estimated to be 0.05 (in blue, simulation ID 11) and 0.23 (in orange, simulation ID 14), respectively. The time-domain waveforms clearly demonstrate the effects of increasing initial orbital eccentric-

¹ We recall that within the quasi-Keplerian parametrization [53, 54] one defines three eccentricities, e_t , e_r and e_ϕ , which can be related to each other by PN expressions. We refer the reader to [52] for details.

² Also called initial mean anomaly in the quasi-Keplerian parametrization [53, 54].

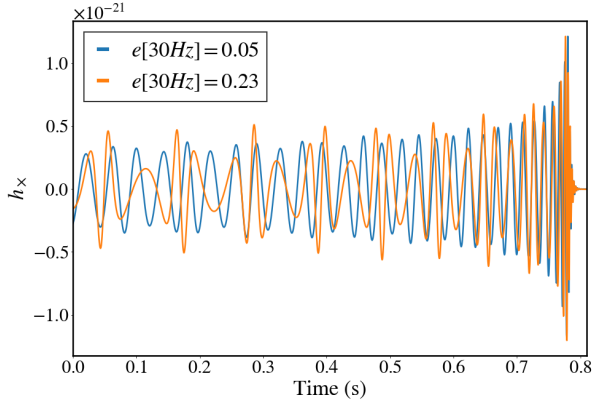


Figure 2: Temporal evolution of the GW polarization state $h_x(t)$ for non-spinning, eccentric stellar-mass binary black holes with total mass $M_T = 50M_\odot$ and mass ratio $q = 2$, provided by numerical-relativity simulations. The characteristic orbital eccentricity of the system—defined at a reference frequency of 30Hz —is estimated to be 0.05 (in blue, simulation ID 11) and 0.23 (in orange, simulation ID 14), respectively.

ity: rapid dephasing, as well as pronounced amplitude modulations due to the advance of the periastron.

III. ANALYSIS

A. Data

The data set used to conduct this study is part of the O2 Data Release through the Gravitational Wave Open Science Center [55]. This covers approximately ≈ 5 days of the coincident data between LIGO Livingston and LIGO Hanford between UTC Interval 2017-02-28 16:30:00 - 2017-03-10 13:35:00. Times with significant instrumental disturbances have been removed from the time period considered here [56, 57]. We consider two search algorithms, PyCBC and cWB, which are described in the following sections.

B. PyCBC : The matched filter algorithm

PyCBC is a search pipeline devised to detect GWs from compact binary coalescences using the PyCBC software package [58]. In this work we have employed the PyCBC search algorithm in a similar configuration as was used for the first catalogue of gravitational waves transients GWTC-1 [1]. For details of the algorithm see [31, 58–61].

In the PyCBC analysis presented here the template bank described in [62] is used. This bank covers binary systems with a total mass between $2M_\odot$ and $500M_\odot$ and mass ratios $q < 98$. Binary components with masses below $2M_\odot$ are assumed to be neutron stars with a maximum dimensionless spin magnitude of 0.05; otherwise the maximum dimensionless spin

magnitude is 0.998. This template bank includes no effects of eccentric orbits.

In a previous study it has been found that a quasicircular bank does not provide a good match for searching binaries with eccentric orbits [63]. Furthermore, it is known that the signal morphology of the eccentric BBH is orthogonal to the aligned-spin quasicircular BBH [64]. As a consequence the template bank, which is restricted to the dominant harmonic of quasicircular non-precessing waveforms, becomes ineffective for searching eccentric BBH with high eccentricities.

The way eccentricity affects the matched-filter search by a quasicircular template bank is twofold, *first* the collection of matched filtered signal-to-noise ratio (SNR) is reduced as a function of eccentricity (this can be quantified by studying the overlap of eccentric and quasicircular waveforms), *second* the signal-based χ^2 veto [59] used for weighting the single detector SNR to compute the rank also penalizes the final detection statistics of the search.

C. cWB : The un-modeled search algorithm

The cWB search pipeline [27, 32, 33] is designed to detect and reconstruct short-lived signals which are weakly modeled or unmodeled using a network of GW detectors [33], but is also effective for signals with a known morphology, as is the case of BBH events reported in GWTC-1 [1].

The configuration of cWB used in this work is the same as used in the GWTC-1 catalog. We refer the reader to [27, 28, 32, 33, 65] for details of the detection process in cWB. The lack of a template bank for binary black holes in eccentric orbits, which could be used by matched filter pipelines, motivated the use of cWB as a robust tool to search eccentric BBH signals during the first and second observing runs of the LIGO and Virgo detectors [28].

The cWB search pipeline performs worse than matched-filter pipelines in the case the signal is well recovered by the template bank. In this case matched-filtering would indeed be the optimal method for Gaussian and stationary noise (these simplifications do however not apply to actual LIGO noise). The sensitivity of cWB significantly improves in parts of the parameter space where the template bank does not faithfully reproduce the incoming signal. In an earlier version of cWB, its search sensitivity was found to have almost no dependency on eccentricity [27]. This was also confirmed in the latest results for observing runs O1 and O2 of the LIGO and Virgo detectors [28]. As a weakly modelled search cWB is more affected by the background noise and hence has a lower sensitivity as compared to matched filter searches for known signals. Nevertheless cWB has been found to provide a valuable complementarity to matched filter searches to detect signals which are outside the template bank, as in the case of eccentric BBH signals [27] or intermediate mass BBH signals [66].

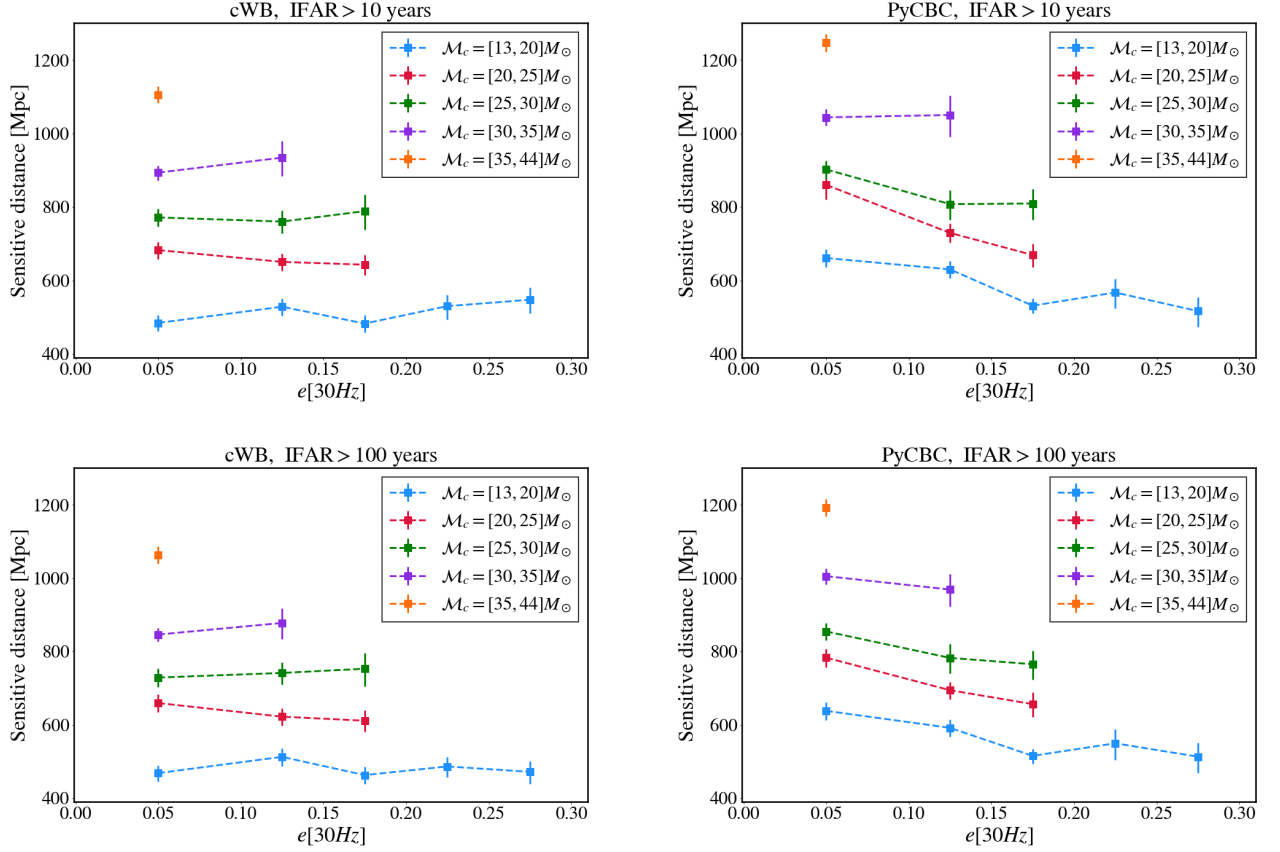


Figure 3: Top row: The left and right panel show the sensitivity range for the cWB and PyCBC search pipelines for various chirp mass bins as a function of eccentricity defined at 30Hz at an IFAR > 10 years, respectively. Bottom row: The left and right panels display the sensitivity range for the cWB and PyCBC search pipeline for various chirp mass bins as a function of eccentricity defined at 30Hz at an IFAR > 100 years, respectively. The plot markers are placed in the center of the eccentricity bins.

IV. SEARCH SENSITIVITY

A. Visible range

The visible range for a given source parameters is calculated by injecting simulated waveforms into the data [31, 32, 61]. The False Alarm Rate (FAR) is a statistic measuring the frequency with which the search would rank non-astrophysical events with a detection statistic comparable to the one of a candidate event. In practice, each recovered signal is assigned an inverse false alarm rate (IFAR=1/FAR) according to its detection statistic. Then, one can compute for each bin of the source parameters the visible volume over a certain IFAR threshold. For a generic binary, the sensitive volume V of a network of detectors with a given sensitivity can be defined as

$$V(\xi) = \int_0^\infty f(z|\xi) \frac{dV_c}{dz} \frac{1}{1+z} dz, \quad (4.1)$$

where $f(z|\xi)$ is the detection probability of a binary with a given parameter set ξ at redshift z , averaged over the extrinsic binary orientation parameters [67]. In Eq. (4.1) the sensitivity

is assumed to be constant over the observing time, T_{obs} , which is why we have chosen the specific chunk of O2 data where sensitivity was almost uniform.

Given a population with parameters θ , the total observed volume can be computed as

$$V_\theta = \int_\xi p(\xi|\theta) V(\xi) d\xi, \quad (4.2)$$

where $p(\xi|\theta)$ describes the underlying distribution of the intrinsic parameters. The visible range can be then estimated as the radius of the visible volume.

The sensitivity of GW searches is a strongly dependent function of the binary chirp mass and distance, and it also varies with spin. We also note that the eccentricity can be a relevant factor depending on the pipeline used to conduct the search. Thus, we have mainly chosen chirp mass binning to study the impact of eccentricity on visible range as it shows more clearly the dependence of the search sensitivity than other parameters, like the total mass.

B. Injection set

The injection set used in this study is composed of the NR waveforms listed in Table I. As a consequence, injections have fixed spin vectors and mass ratio values corresponding to those of the NR waveforms. Nonetheless, the total mass of the system acts as a scale parameter which can be freely specified, subject only to consistency with the length of the NR waveforms such that the injected signals start at the specified starting frequency in the band of the detectors. Due to the length limitations of the NR waveforms we set the starting frequency of the injection set to 30Hz , which is also the frequency at which the value of eccentricity is specified.

We have chosen the number of performed injections to limit the computational cost necessary to run the search pipelines. We note that PyCBC is more expensive than cWB, however it also allows to achieve higher IFAR values. The largest subset of injected waveforms corresponds to $q = 1$ nonspinning with 17317 injections distributed among cases with IDs 1, 2, 3 and 4 in Table I. While the number of injections for the rest of waveforms has been decreased substantially due to the limited computational resources available to 3591 for $\chi_{\text{eff}} < 0$ cases (IDs 5, 6 and 7), 4723 for $\chi_{\text{eff}} > 0$ configurations (IDs 8, 9 and 10), 6416 for $q = 2$ simulations and 4458 for $q = 4$ simulations (IDs 15, 16 and 17). As a consequence, the equal mass non-spinning eccentric case provides better statistics and permits to clearly identify the behavior of the sensitivity of both pipelines for specific values of chirp mass and eccentricity, as shown in Sec. IV C.

The injection set is constructed using a uniform distribution in distance scaled by the chirp mass [68]. The total mass values are uniformly distributed from a minimum value consistent with the length of the NR waveforms, between $[30 - 50]M_{\odot}$ for our dataset, to a maximum total mass of $100M_{\odot}$.

The orbital eccentricity of the individual injections, defined at a reference frequency of 30Hz is estimated through Eq. (2.3). We note that with this method the maximum eccentricity at 30Hz of a given injected NR waveform is given by the values of the last column of Table I, as these values are measured at the start of the NR waveforms.

The moderate values of eccentricity considered here are well-suited for a first study of the sensitivity of gravitational waves searches to full IMR signals. Furthermore, many astrophysical models for eccentric binary black hole coalescences in the frequency band of ground-based detectors predict similar eccentricity values as those used here [15, 69–71].

C. Effect of eccentricity on search sensitivities

We now turn to discussing the visible range at IFAR thresholds of 10 and 100 years for both search pipelines and the same injection set. Although matched-filter searches are an optimal method to search for signals of known morphologies, in the case of eccentric BBHs computationally efficient waveform models describing the full GW signal of eccentric BBH coalescences have not yet been developed. For this reason it is

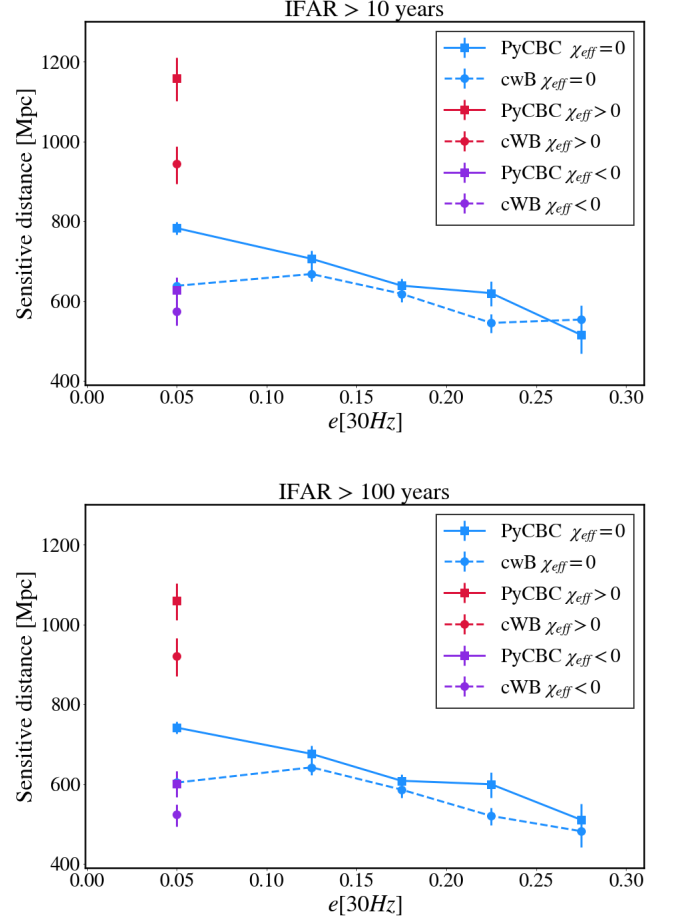


Figure 4: The upper (lower) panel shows the sensitivity range for the cWB and PyCBC search pipelines for equal mass non-spinning, positive spins and negative spins as a function of eccentricity defined at 30Hz at an $\text{IFAR} > 10$ years ($\text{IFAR} > 100$ years). The plot markers are placed in the center of the eccentricity bins.

expected that the quasicircular template bank used by PyCBC will not be able to detect eccentric BBH events with orbital eccentricities beyond a certain threshold. On the other hand, cWB does not require signal models for detection and thus its sensitivity to eccentric BBH signals is expected to only vary significantly as a function of signal strength, but only weakly in terms of other parameters like eccentricity. It should be noted, however, that cWB is not an optimal method to detect BBH merger events and thus has lower sensitivity than PyCBC for regions of parameter space which are either explicitly covered by the PyCBC template bank or where the signal is otherwise ‘mimicked’ by templates in the bank.

In Figure 3 we exhibit the visible ranges of the PyCBC and cWB pipelines binned in chirp mass and eccentricity for all the injected signals. The results show a reduction in visible range of PyCBC with increasing eccentricity. The steepness of the reduction of visible range becomes more apparent when one goes to lower chirp masses; this is due to the fact that for high chirp masses the number of cycles visible in the sen-

sitivity band of the LIGO detectors (and hence the inspiral part of the signal where eccentricity effects are pronounced) is rather short. One can conclude that for high chirp mass events with moderate to low eccentricities the PyCBC search and its quasicircular template bank does not lose much visible range. This behaviour is contrary to the low chirp mass case with moderate eccentricities, where the loss in visible range is substantial.

ID	$M_T [M_\odot]$	$D_L [\text{Mpc}]$	e_{inj}	\mathcal{M}^{Ecc}	\mathcal{M}^{QC}
9	46.4	277	0.11	0.95	0.86
12	96.4	200	0.04	0.98	0.93

Table II: Summary of the injected signals in Fig. 5. The first column denotes the identifier of the simulation. The next columns indicate the total mass, M_T , the luminosity distance, D_L , the eccentricity, e_{inj} , of the injection, the match between the injected signal and the recovered one by cWB, \mathcal{M}^{Ecc} , and the match between the injected signal and the QC template with the same injected parameters, \mathcal{M}^{QC} .

Regarding cWB, previous work [28] found that the search pipeline is almost independent of eccentricity for a given chirp mass bin. However, the waveforms used in that investigation [72] were based on geodesics in Kerr spacetime and the quadrupole formula for energy loss, and significantly less accurate than the NR simulations used here.

We note an interesting feature in the dependency of the range as a function of eccentricity for cWB for the lowest chirp mass bin at IFAR > 10 years. The range increases slightly as a function of eccentricity. This might probably be attributed to the power content in higher harmonics in eccentric BBH signals which is enhanced when the eccentricity increases. cWB captures the total excess power in the network of detectors and therefore can observe eccentric BBH events at larger range. However, we note that this particular small increase in sensitivity is also compatible with a constant sensitive distance as the values are within the statistical error bars. We find that our results are robust when changing the IFAR threshold from 10 to 100 years: sensitivity results for the higher IFAR choice are shown in the lower panels of Fig. 3. One observes the expected overall decrease of the sensitive distance of both pipelines with increasing IFAR. Moreover, it can be noted that the dependence of the visible range on eccentricity retains the same features as at IFAR > 10 years for both pipelines.

In our NR simulations we only have waveforms with moderate eccentricities ($e_{30\text{Hz}} < 0.3$). The subset of spinning waveforms is even more restricted in eccentricity values ($e_{30\text{Hz}} < 0.12$). As a consequence, a study of the impact of the effect of eccentricity and spins is more difficult. In Fig. 4 we show the sensitive distance for the equal mass spinning and non-spinning eccentric waveforms as a function of eccentricity for the chirp mass bin $[13, 30] M_\odot$. As expected, one observes that PyCBC has larger sensitivity for positive spins than for negative spins, as for positive spins the matched filter pipeline can collect more SNR than for negative spins. There is also a drop in sensitivity for PyCBC with increasing eccentricity,

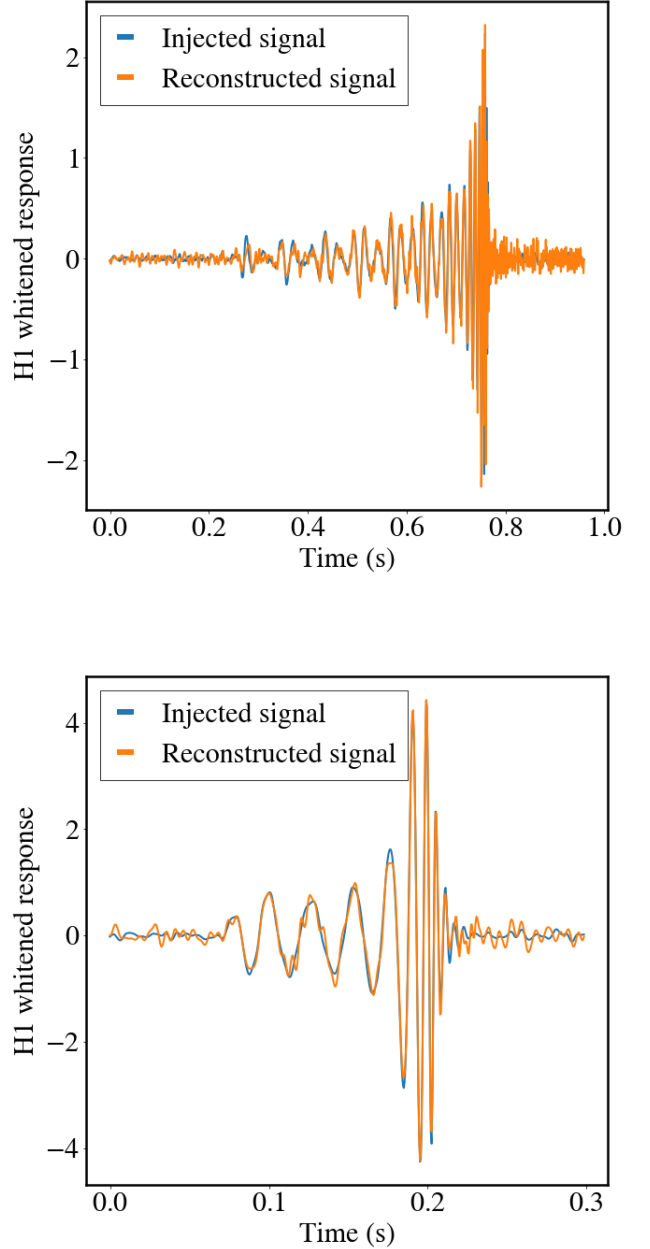


Figure 5: In the upper and lower panels the whitened detector response of LIGO Hanford, H1, in time domain are displayed for an injected signal corresponding to the waveform with ID 9 and 12 from Table I, respectively. Some of the parameters of the injected signals are shown in Table II. In both panels the injected and reconstructed signals are represented with blue and orange colors, respectively.

while for cWB the small drop in sensitivity is consistent with statistical error bars. We note here that the results for the spinning waveforms are computed over a smaller number of injections compared to the nonspinning case, as explained in Sec. IV B. In addition the small range in eccentricity of the spinning simulation does not allow to identify specific trends for

the sensitivity as a function of the eccentricity. We point out that more insightful results could be obtained by increasing the number of injections and the range of values of initial eccentricity of the waveforms, and we leave the study of a large parameter space of the eccentric non-precessing spin sector, as well as eccentric spin-precessing systems, to future work.

Finally, we illustrate an example of the robust waveform reconstruction procedure of cWB [73] applied to eccentric signals. In Fig. 5 we display the whitened detector response of LIGO Hanford (H1) to two eccentric injected signals and the corresponding reconstructed waveforms by cWB, specifically for injections corresponding to the cases with ID 9 and 12 from Table I, with injection parameters specified in Table II. We have also calculated the match, defined as the noise weighted inner product [74], between the injected and recovered signal with cWB obtaining high agreement between both. The results of the match are also reported for a quasicircular template waveform computed against the same injected signals. One observes that the match against the quasicircular template, calculated using the SEOBNRv4 waveform model [75], decreases significantly with increasing eccentricity, from $\mathcal{M} = 0.93$ for ID 12 to $\mathcal{M} = 0.85$ for ID 9, while the drop in the match against the cWB reconstructed waveform goes from $\mathcal{M} = 0.98$ for ID 12 to $\mathcal{M} = 0.95$ for ID 9. For cWB the match decreases because the signal with ID 9 is longer than for ID 12, and the reconstruction is expected to degrade the longer the signal is, while for the quasicircular template the increase of eccentricity decreases substantially the match due to the inability to resemble eccentric features in the injected signal.

It should also be remarked that for cWB as an unmodelled search algorithm a high match between reconstructed and injected signal does not directly translate into having a high sensitivity of the pipeline as it is not a matched filter search pipeline. However, from a waveform modelling perspective it is still relevant to observe the ability of cWB to reconstruct the eccentric signal and the inability of the quasicircular template to resemble the injected signal with increasing eccentricity. As expected the reconstructed signal degrades after the waveform peak, thus, the ringdown is poorly reproduced due to the decrease in power of the signal. With these examples we want to illustrate the capability of cWB to recover features of eccentric signals, and we leave a thorough analysis of the reconstruction procedure of cWB applied to eccentric BBH signals for future work.

D. Comparisons of search sensitivities and astrophysical implications

In Figure 6 we show the comparison of the visible volumes of PyCBC and cWB at IFAR thresholds of 10 and 100 years. Within our injection set PyCBC almost always performs better than or similar to cWB in terms of visible volume. In the case of low chirp mass and high eccentricity the situation is reversed: PyCBC loses sensitivity and cWB becomes more sensitive, specially at IFAR > 10 years.

In the lower panel of Fig. 6 the comparison in sensitive vol-

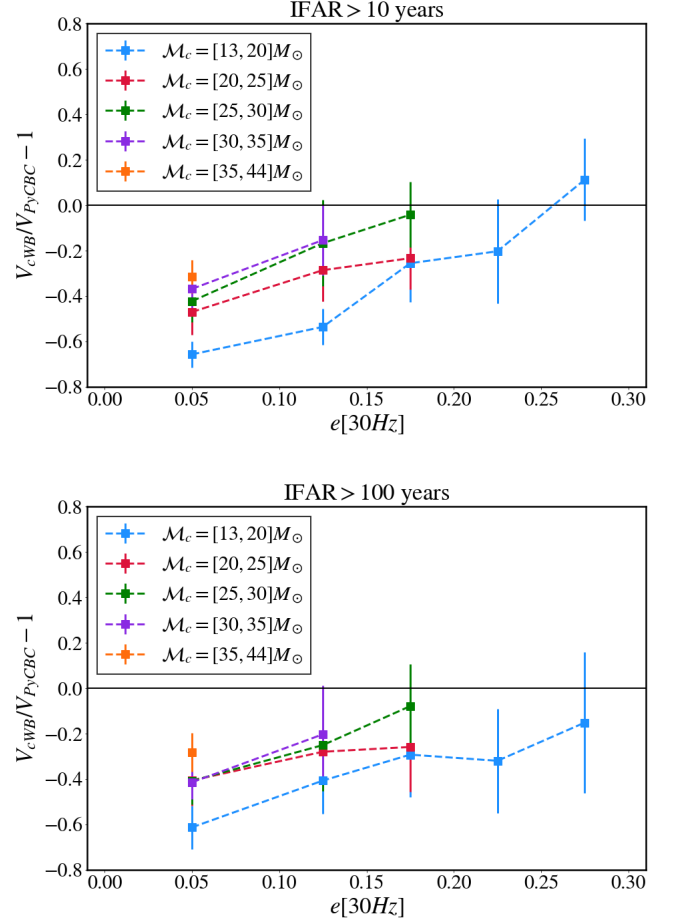


Figure 6: In the upper (lower) panel the relative difference in sensitivity volume between the search sensitivity of pyCBC and cWB for various chirp mass bins is presented as function of eccentricity at an IFAR > 10 (IFAR > 100) years. The plot markers are placed in the center of the eccentricity bins.

ume between both pipelines at IFAR > 100 years is shown. One observes that the trends in relative volume between both pipelines are similar to the case at an IFAR threshold of 10 years, although the error estimates are larger due to the decrease in sensitivity of both pipelines with increasing IFAR values. The results show that PyCBC has a larger sensitive volume than cWB, even for the low chirp mass bin. However, with increasing eccentricity the decrease in sensitive volume of PyCBC and the constancy of the cWB one, make the relative volume to be an increasing function, which for higher values of eccentricity is expected to cross zero, as it is the case at IFAR > 10 years.

These comparison results can also be viewed in the light of coalescence rate. Suppose the coalescence rate of eccentric BBH mergers with eccentricities between (0, 0.3) at 30 Hz is R_{eBBH} ; then the number of visible events will be simply $N_{events} = R_{eBBH} \times V_{iFAR} \times T_{obs}$. The relative difference in the number of detected events will be the same as the relative difference between the visible volume for the two search algo-

rithms that we have considered. From this, we can conclude that at IFAR > 10 years cWB will see $\sim 10\%$ more events than PyCBC if the chirp mass is between $[13M_{\odot}, 20M_{\odot}]$ and the eccentricity at 30 Hz is between $[0.25-0.3]$.

V. CONCLUSIONS

In this paper we have quantified for the first time the sensitivities of GW search algorithms to eccentric BBH signals, using NR simulations of eccentric BBH mergers. The effect of eccentricity on matched filtered searches has only been studied for inspiral-only waveforms until now [63]; we have extended those studies to complete IMR signals. The search range of unmodeled searches for eccentric signals has been previously investigated with a particular IMR waveform model [28]; however, that waveform model is far less accurate than the NR simulations used here.

We have employed two different gravitational wave searches for BBHs to compare the search sensitivity in terms of visible volume. The matched filter search PyCBC performs better than the unmodeled search cWB in most parts of the limited parameter space that we have considered. Only in the parameter space region of low chirp mass and high eccentricity does cWB perform better than PyCBC. It should also be noted that the parameter space that is covered by our NR injections is rather small. Due to the restricted length of the NR simulations, the parameter space of low chirp mass ($M_c < 13$) and high eccentricity $e_{30\text{Hz}} > 0.3$ is not yet probed in this work. This, however, is the most interesting part of parameter space for eccentric BBHs, with waveform morphologies that are substantially different than those of quasicircular BBHs. We plan to investigate this part of parameter space in subsequent work, with eccentric hybrid waveforms that combine NR data with an analytic description of the inspiral, or with future waveform models for the full IMR signal.

The two search pipelines used here —very different algorithms as described in Sec. III— offer a complementary way to search for BBH mergers in different parts of the source parameter space. Constructing a template-based search for eccentric BBH will be challenging as the rate of background triggers increases with the increase of template bank parameters. In the light of astrophysical considerations [14, 15], most of the BBH events observable by LIGO and Virgo are expected to have eccentricities lower than 0.2 at 30 Hz; this region of parameter space has been demonstrated to be well-covered by the PyCBC search, even with a quasi-circular template bank. Certain astrophysical scenarios suggest LIGO-Virgo relevant BBH events with higher eccentricities: for such sources the cWB search provides decent coverage.

With the expected availability of computationally efficient and accurate eccentric IMR BBH waveform models (and/or eccentric hybrids) in the near future it will be interesting to probe the low chirp mass and high eccentricity part of the parameter space, where the modelled search is penalized due to substantial dephasing between the quasicircular template bank and the signal.

With future upgrades [76], the detectors' low-frequency

sensitivity (in the range 24 – 100 Hz) is expected to improve significantly; this will in turn allow a significant gain in SNR during the inspiral even for BBH systems with relatively high masses, adding more prominence to detectable inspiral features like eccentricity and penalizing the matched-filter searches for eccentric BBH even further. With future improvements at low frequencies, the role of un-modeled searches is therefore expected to become important also for the part of parameter space which is well-covered by matched-filter searches at current detector configuration.

VI. ACKNOWLEDGEMENTS

We would like to thank Debnandini Mukherjee for useful comments about the manuscript. This work was supported by the Spanish Ministry of Education and Professional Formation grants FPU15/03344. The author also acknowledges the support by the Govern de les Illes Balears through the Vicepresidència i Conselleria d'Innovació, Recerca i Turisme and the Direcció General de Política Universitària i Recerca with funds from the Tourist Stay Tax Law ITS 2017-006 (PRD2018/24), the European Union FEDER funds and EU COST Actions CA18108, CA17137, CA16214, and CA16104, the Ministry of Science, Innovation and Universities and the Spanish Agencia Estatal de Investigación grants FPA2016-76821-P, RED2018-102661-T, RED2018-102573-E, FPA2017-90566-REDC, FPA2017-90687-REDC, and the Generalitat Valenciana (PROMETEO/2019/071). The author thankfully acknowledges the computer resources at MareNostrum and the technical support provided by Barcelona Supercomputing Center (BSC) through Grants No. AECT-2020-1-0025, AECT-2019-3-0020, AECT-2019-2-0010, AECT-2019-1-0022, AECT-2018-3-0017, AECT-2018-2-0022, AECT-2018-1-0009, AECT-2017-3-0013, AECT-2017-2-0017, AECT2017-1-0017, AECT-2016-3-0014, AECT2016-2-0009, from the Red Española de Supercomputación (RES) and PRACE (Grant No. 2015133131). ET simulations were carried out on the BSC MareNostrum computer center under PRACE and RES allocations and on the FONER cluster at the University of the Balearic Islands. The authors are grateful for computational resources provided by the LIGO Laboratory and supported by National Science Foundation Grants PHY-0757058 and PHY-0823459. MH acknowledges support from Swiss National Science Foundation (SNSF) grant IZCOZ0-177057. ARB is grateful to the Pauli Center for Theoretical Studies at ETHZ which provided valuable travel support during stages of this work. S.T. is supported by Forschungskredit Nr. FK-19-114 and Swiss National Science Foundation grant number 200020 182047. This research has made use of data, software and/or web tools obtained from the Gravitational Wave Open Science Center (<https://www.gw-openscience.org>), a service of LIGO Laboratory, the LIGO Scientific Collaboration and the Virgo Collaboration. LIGO is funded by the U.S. National Science Foundation. Virgo is funded by the French Centre National de Recherche Scientifique (CNRS), the Italian Istituto Nazionale della Fisica Nucleare (INFN) and the Dutch Nikhef, with con-

tributions by Polish and Hungarian institutes. The authors gratefully acknowledge the support of the NSF CIT cluster

for the provision of computational resources for pyCBC and cWB runs.

-
- [1] B. P. Abbott et al. GWTC-1: A Gravitational-Wave Transient Catalog of Compact Binary Mergers Observed by LIGO and Virgo during the First and Second Observing Runs. *Phys. Rev.*, X9(3):031040, 2019.
 - [2] <https://gracedb.ligo.org/superevents/public/O3/>.
 - [3] B.P. Abbott et al. GW190425: Observation of a Compact Binary Coalescence with Total Mass $\sim 3.4M_{\odot}$. *Astrophys. J. Lett.*, 892:L3, 2020.
 - [4] R. Abbott et al. GW190412: Observation of a Binary-Black-Hole Coalescence with Asymmetric Masses. 4 2020.
 - [5] LIGO Scientific Collaboration and Virgo Collaboration. GWTC-2. In preparation. 2020.
 - [6] B. P. Abbott et al. Search for Eccentric Binary Black Hole Mergers with Advanced LIGO and Advanced Virgo during their First and Second Observing Runs. 2019.
 - [7] Isobel M. Romero-Shaw, Paul D. Lasky, and Eric Thrane. Searching for Eccentricity: Signatures of Dynamical Formation in the First Gravitational-Wave Transient Catalogue of LIGO and Virgo. *Mon. Not. Roy. Astron. Soc.*, 490(4):5210–5216, 2019.
 - [8] Hans A. Bethe and G. E. Brown. Evolution of binary compact objects which merge. *Astrophys. J.*, 506:780–789, 1998.
 - [9] Krzysztof Belczynski, Vassiliki Kalogera, and Tomasz Bulik. A comprehensive study of binary compact objects as gravitational wave sources: Evolutionary channels, rates, and physical properties. *The Astrophysical Journal*, 572(1):407–431, jun 2002.
 - [10] Matthias U Kruckow, Thomas M Tauris, Norbert Langer, Michael Kramer, and Robert G Izzard. Progenitors of gravitational wave mergers: binary evolution with the stellar grid-based code ComBinE. *Monthly Notices of the Royal Astronomical Society*, 481(2):1908–1949, 08 2018.
 - [11] Jim W. Barrett, Sebastian M. Gaebel, Coenraad J. Neijssel, Alejandro Vigna-Gómez, Simon Stevenson, Christopher P. L. Berry, Will M. Farr, and Ilya Mandel. Accuracy of inference on the physics of binary evolution from gravitational-wave observations. *Mon. Not. Roy. Astron. Soc.*, 477(4):4685–4695, 2018.
 - [12] P. C. Peters and J. Mathews. Gravitational radiation from point masses in a keplerian orbit. *Phys. Rev.*, 131:435–440, Jul 1963.
 - [13] P. C. Peters. Gravitational radiation and the motion of two point masses. *Phys. Rev.*, 136:B1224–B1232, Nov 1964.
 - [14] Ryan M. O’Leary, Frederic A. Rasio, John M. Fregeau, Natalia Ivanova, and Richard O’Shaughnessy. Binary mergers and growth of black holes in dense star clusters. *The Astrophysical Journal*, 637(2):937–951, feb 2006.
 - [15] Johan Samsing. Eccentric black hole mergers forming in globular clusters. *Phys. Rev. D*, 97:103014, May 2018.
 - [16] Giacomo Fragione and Bence Kocsis. Black hole mergers from quadruples. *Mon. Not. Roy. Astron. Soc.*, 486(4):4781–4789, 2019.
 - [17] Jun Kumamoto, Michiko S. Fujii, and Ataru Tanikawa. Gravitational-Wave Emission from Binary Black Holes Formed in Open Clusters. *Mon. Not. Roy. Astron. Soc.*, 486(3):3942–3950, 2019.
 - [18] Ryan M. O’Leary, Bence Kocsis, and Abraham Loeb. Gravitational waves from scattering of stellar-mass black holes in galactic nuclei. *Mon. Not. Roy. Astron. Soc.*, 395(4):2127–2146, 2009.
 - [19] J. Aasi et al. Advanced LIGO. *Class. Quant. Grav.*, 32:074001, 2015.
 - [20] F. Acernese et al. Advanced Virgo: a second-generation interferometric gravitational wave detector. *Class. Quant. Grav.*, 32(2):024001, 2015.
 - [21] B. P. Abbott et al. Binary Black Hole Population Properties Inferred from the First and Second Observing Runs of Advanced LIGO and Advanced Virgo. *Astrophys. J.*, 882(2):L24, 2019.
 - [22] Ilya Mandel and Richard O’Shaughnessy. Compact Binary Coalescences in the Band of Ground-based Gravitational-Wave Detectors. *Class. Quant. Grav.*, 27:114007, 2010.
 - [23] B. P. Abbott et al. Astrophysical Implications of the Binary Black-Hole Merger GW150914. *Astrophys. J.*, 818(2):L22, 2016.
 - [24] Will M. Farr, Simon Stevenson, M. Coleman Miller, Ilya Mandel, Ben Farr, and Alberto Vecchio. Distinguishing Spin-Aligned and Isotropic Black Hole Populations With Gravitational Waves. *Nature*, 548:426, 2017.
 - [25] M.L. Lidov. The evolution of orbits of artificial satellites of planets under the action of gravitational perturbations of external bodies. *Planetary and Space Science*, 9(10):719 – 759, 1962.
 - [26] Yoshihide Kozai. Secular perturbations of asteroids with high inclination and eccentricity. *Astron. J.*, 67:591–598, 1962.
 - [27] V. Tiwari, S. Klimentenko, N. Christensen, E. A. Huerta, S. R. P. Mohapatra, A. Gopakumar, M. Haney, P. Ajith, S. T. McWilliams, G. Vedovato, M. Drago, F. Salemi, G. A. Prodi, C. Lazzaro, S. Tiwari, G. Mitselmakher, and F. Da Silva. Proposed search for the detection of gravitational waves from eccentric binary black holes. *Phys. Rev. D*, 93:043007, Feb 2016.
 - [28] B. P. Abbott and et al. Search for eccentric binary black hole mergers with advanced LIGO and advanced virgo during their first and second observing runs. *The Astrophysical Journal*, 883(2):149, sep 2019.
 - [29] Alexander H. Nitz, Amber Lenon, and Duncan A. Brown. Search for Eccentric Binary Neutron Star Mergers in the first and second observing runs of Advanced LIGO. *Astrophys. J.*, 890:1, 12 2019.
 - [30] Bruce Allen, Warren G. Anderson, Patrick R. Brady, Duncan A. Brown, and Jolien D. E. Creighton. Findchirp: An algorithm for detection of gravitational waves from inspiraling compact binaries. *Phys. Rev. D*, 85:122006, Jun 2012.
 - [31] Samantha A. Usman et al. The PyCBC search for gravitational waves from compact binary coalescence. *Class. Quant. Grav.*, 33(21):215004, 2016.
 - [32] S. Klimentenko, I. Yakushin, A. Mercer, and Guenakh Mitselmakher. Coherent method for detection of gravitational wave bursts. *Class. Quant. Grav.*, 25:114029, 2008.
 - [33] S. Klimentenko, G. Vedovato, M. Drago, F. Salemi, V. Tiwari, G. A. Prodi, C. Lazzaro, K. Ackley, S. Tiwari, C. F. Da Silva, and G. Mitselmakher. Method for detection and reconstruction of gravitational wave transients with networks of advanced detectors. *Phys. Rev. D*, 93:042004, Feb 2016.
 - [34] B. S. Sathyaprakash and B. F. Schutz. Physics, Astrophysics and Cosmology with Gravitational Waves. *Living Rev. Rel.*, 12:2, 2009.
 - [35] Lee Samuel Finn and David F. Chernoff. Observing binary in-

- spiral in gravitational radiation: One interferometer. *Phys. Rev. D*, 47:2198–2219, Mar 1993.
- [36] Piotr Jaranowski, Andrzej Królak, and Bernard F. Schutz. Data analysis of gravitational-wave signals from spinning neutron stars: The signal and its detection. *Phys. Rev. D*, 58:063001, Aug 1998.
- [37] Frank Löffler et al. The Einstein Toolkit: A Community Computational Infrastructure for Relativistic Astrophysics. *Class. Quant. Grav.*, 29:115001, 2012.
- [38] Maria Babiuc-Hamilton et al. The Einstein Toolkit, October 2019. To find out more, visit <http://einstein toolkit.org>.
- [39] SXS collaboration. <https://www.black-holes.org/SpEC.html>.
- [40] Antoni Ramos-Buades, Sascha Husa, Geraint Pratten, Héctor Estellés, Cecilio García-Quirós, Maite Mateu-Lucena, Marta Colleoni, and Rafel Jaume. First survey of spinning eccentric black hole mergers: Numerical relativity simulations, hybrid waveforms, and parameter estimation. *Phys. Rev. D*, 101(8):083015, 2020.
- [41] Ian Hinder, Lawrence E. Kidder, and Harald P. Pfeiffer. Eccentric binary black hole inspiral-merger-ringdown gravitational waveform model from numerical relativity and post-newtonian theory. *Phys. Rev. D*, 98:044015, Aug 2018.
- [42] V. Tiwari, S. Klimentko, N. Christensen, E. A. Huerta, S. R. P. Mohapatra, A. Gopakumar, M. Haney, P. Ajith, S. T. McWilliams, G. Vedovato, M. Drago, F. Salemi, G. A. Prodi, C. Lazzaro, S. Tiwari, G. Mitselmakher, and F. Da Silva. Proposed search for the detection of gravitational waves from eccentric binary black holes. *Phys. Rev. D*, 93:043007, Feb 2016.
- [43] Sascha Husa, Mark Hannam, Jose A. Gonzalez, Ulrich Sperhake, and Bernd Bruegmann. Reducing eccentricity in black-hole binary evolutions with initial parameters from post-Newtonian inspiral. *Phys. Rev.*, D77:044037, 2008.
- [44] Harald P. Pfeiffer, Duncan A. Brown, Lawrence E. Kidder, Lee Lindblom, Geoffrey Lovelace, and Mark A. Scheel. Reducing orbital eccentricity in binary black hole simulations. *Class. Quant. Grav.*, 24:S59–S82, 2007.
- [45] Wolfgang Tichy and Pedro Marronetti. A Simple method to set up low eccentricity initial data for moving puncture simulations. *Phys. Rev.*, D83:024012, 2011.
- [46] Alessandra Buonanno, Lawrence E. Kidder, Abdul H. Mroue, Harald P. Pfeiffer, and Andrea Taracchini. Reducing orbital eccentricity of precessing black-hole binaries. *Phys. Rev.*, D83:104034, 2011.
- [47] Abdul H. Mroue, Harald P. Pfeiffer, Lawrence E. Kidder, and Saul A. Teukolsky. Measuring orbital eccentricity and periastron advance in quasi-circular black hole simulations. *Phys. Rev.*, D82:124016, 2010.
- [48] Michael Pürrer, Sascha Husa, and Mark Hannam. An efficient iterative method to reduce eccentricity in numerical-relativity simulations of compact binary inspiral. *Phys. Rev. D*, 85(12), Jun 2012.
- [49] Antoni Ramos-Buades, Sascha Husa, and Geraint Pratten. Simple procedures to reduce eccentricity of binary black hole simulations. *Phys. Rev. D*, 99:023003, Jan 2019.
- [50] Miriam Cabero, Alex B. Nielsen, Andrew P. Lundgren, and Collin D. Capano. Minimum energy and the end of the inspiral in the post-newtonian approximation. *Phys. Rev. D*, 95:064016, Mar 2017.
- [51] Héctor Estellés, Antoni Ramos-Buades, Sascha Husa, Cecilio García-Quirós, Marta Colleoni, Leila Haegel, and Rafel Jaume. IMRPhenomTP: A phenomenological time domain model for dominant quadrupole gravitational wave signal of coalescing binary black holes. 4 2020.
- [52] K. G. Arun, Luc Blanchet, Bala R. Iyer, and Siddhartha Sinha. Third post-newtonian angular momentum flux and the secular evolution of orbital elements for inspiralling compact binaries in quasi-elliptical orbits. *Phys. Rev. D*, 80:124018, Dec 2009.
- [53] T. Damour and N. Deruelle. General relativistic celestial mechanics of binary systems. I. The post-Newtonian motion. *Ann. Inst. Henri Poincaré Phys. Théor.*, Vol. 43, No. 1, p. 107 - 132, 1985.
- [54] Raoul-Martin Memmesheimer, Achamveedu Gopakumar, and Gerhard Schafer. Third post-Newtonian accurate generalized quasi-Keplerian parametrization for compact binaries in eccentric orbits. *Phys. Rev.*, D70:104011, 2004.
- [55] Rich Abbott et al. Open data from the first and second observing runs of Advanced LIGO and Advanced Virgo. 12 2019.
- [56] B P Abbott et al. Characterization of transient noise in advanced LIGO relevant to gravitational wave signal GW150914. *Classical and Quantum Gravity*, 33(13):134001, jun 2016.
- [57] J. Aasi et al. The characterization of Virgo data and its impact on gravitational-wave searches. *Class. Quant. Grav.*, 29:155002, 2012.
- [58] Samantha A. Usman, Alexander H. Nitz, Ian W. Harry, Christopher M. Biwer, Duncan A. Brown, Miriam Cabero, Collin D. Capano, Tito Dal Canton, Thomas Dent, Stephen Fairhurst, Marcel S. Kehl, Drew Keppel, Badri Krishnan, Amber Lenon, Andrew Lundgren, Alex B. Nielsen, Larne P. Pekowsky, Harald P. Pfeiffer, Peter R. Saulson, Matthew West, and Joshua L. Willis. The PyCBC search for gravitational waves from compact binary coalescence. *Classical and Quantum Gravity*, 33(21):215004, November 2016.
- [59] Bruce Allen. χ^2 time-frequency discriminator for gravitational wave detection. *Phys. Rev. D*, 71:062001, Mar 2005.
- [60] Bruce Allen, Warren G. Anderson, Patrick R. Brady, Duncan A. Brown, and Jolien D. E. Creighton. Findchirp: An algorithm for detection of gravitational waves from inspiralling compact binaries. *Phys. Rev. D*, 85:122006, Jun 2012.
- [61] Alexander H. Nitz, Thomas Dent, Tito Dal Canton, Stephen Fairhurst, and Duncan A. Brown. Detecting binary compact-object mergers with gravitational waves: Understanding and improving the sensitivity of the PyCBC search. *The Astrophysical Journal*, 849(2):118, nov 2017.
- [62] Tito Dal Canton and Ian W. Harry. Designing a template bank to observe compact binary coalescences in Advanced LIGO’s second observing run. *arXiv e-prints*, page arXiv:1705.01845, May 2017.
- [63] Duncan A. Brown and Peter J. Zimmerman. Effect of eccentricity on searches for gravitational waves from coalescing compact binaries in ground-based detectors. *Phys. Rev. D*, 81:024007, Jan 2010.
- [64] E. A. Huerta, C. J. Moore, Prayush Kumar, Daniel George, Alvin J. K. Chua, Roland Haas, Erik Wessel, Daniel Johnson, Derek Glennon, Adam Rebei, A. Miguel Holgado, Jonathan R. Gair, and Harald P. Pfeiffer. Eccentric, nonspinning, inspiral, gaussian-process merger approximant for the detection and characterization of eccentric binary black hole mergers. *Phys. Rev. D*, 97:024031, Jan 2018.
- [65] V. Tiwari, S. Klimentko, V. Necula, and G. Mitselmakher. Reconstruction of chirp mass in searches for gravitational wave transients. *Classical and Quantum Gravity*, 33(1):01LT01, January 2016.
- [66] Juan Calderón Bustillo, Francesco Salemi, Tito Dal Canton, and Karan P. Jani. Sensitivity of gravitational wave searches to the full signal of intermediate-mass black hole binaries during the first observing run of Advanced LIGO. *Phys. Rev. D*, 97(2):024016, 2018.
- [67] B. P. Abbott and et al. Binary black hole population proper-

- ties inferred from the first and second observing runs of advanced LIGO and advanced virgo. *The Astrophysical Journal*, 882(2):L24, sep 2019.
- [68] Vaibhav Tiwari. Estimation of the sensitive volume for gravitational-wave source populations using weighted Monte Carlo integration. *Classical and Quantum Gravity*, 35(14):145009, July 2018.
- [69] F. Antonini, S. Chatterjee, C. L. Rodriguez, M. Morscher, B. Pattabiraman, V. Kalogera, and F. A. Rasio. Black Hole Mergers and Blue Stragglers from Hierarchical Triples Formed in Globular Clusters. *Astrophys. J.*, 816:65, January 2016.
- [70] F. Antonini and F. A. Rasio. Merging Black Hole Binaries in Galactic Nuclei: Implications for Advanced-LIGO Detections. *Astrophys. J.*, 831:187, November 2016.
- [71] L. Gondán, B. Kocsis, P. Raffai, and Z. Frei. Eccentric Black Hole Gravitational-wave Capture Sources in Galactic Nuclei: Distribution of Binary Parameters. *Astrophys. J.*, 860:5, June 2018.
- [72] William E. East, Sean T. McWilliams, Janna Levin, and Frans Pretorius. Observing complete gravitational wave signals from dynamical capture binaries. *Phys. Rev. D*, 87(4):043004, 2013.
- [73] F. Salemi, E. Milotti, G.A. Prodi, G. Vedovato, C. Lazzaro, S. Tiwari, S. Vinciguerra, M. Drago, and S. Klimenko. Wider look at the gravitational-wave transients from GWTC-1 using an unmodeled reconstruction method. *Phys. Rev. D*, 100(4):042003, 2019.
- [74] Piotr Jaranowski and Andrzej Królak. Gravitational-wave data analysis. formalism and sample applications: The gaussian case. *Living Reviews in Relativity*, 15(1):4, Mar 2012.
- [75] Alejandro Bohé et al. Improved effective-one-body model of spinning, nonprecessing binary black holes for the era of gravitational-wave astrophysics with advanced detectors. *Phys. Rev.*, D95(4):044028, 2017.
- [76] J. Aasi et al. Prospects for Localization of Gravitational Wave Transients by the Advanced LIGO and Advanced Virgo Observatories. 2013.